Journal of the Korean Society of Remote Sensing, Vol. 10, No. 2, 1994

Navigation and Fine Co-location of ATSR Images

DONGSEOK SHIN and JOHN K. POLLARD

Electronic and Electrical Engineering Department
University College London
Torrington Place, London, WC1E 7JE, U.K.

TEL : +44-171-419-3946
FAX : +44-171-387-4350

Abstract

In this paper, we propose a comprehensive geometric correction algorithm of Along Track Scanning Radiometer(ATSR) images. The procedure consists of two cascaded modules; pre-correction and fine co-location.

The pre-correction algorithm is based on the navigation model which was derived in mathematical forms. This model was applied for correcting raw (un-geolocated) ATSR images. The non-systematic geometric errors are also introduced as the limitation of the geometric correction by this analytical method.

A fast and automatic algorithm is also presented in this paper for co-locating nadir and forward views of the ATSR images by using a *binary cross-correlation matching* technique. It removes small non-systematic errors which cannot be corrected by the analytic method. The proposed algorithm does not require any auxiliary information, or *a priori* knowledge. Single channel thermal IR data ($11\mu m$) are used for this algorithm giving faster processing and avoiding the imperfect co-registration problem observed with multiple channels. Coastlines in images are detected by a region segmentation and an automatic thresholding technique. The matching procedure is carried out with binary coastline images (nadir and forward), and it gives comparable accuracy and faster processing than a patch based matching technique. This technique automatically reduces non-systematic errors between two views to ± 1 pixel.

1 Introduction

A space world above Korea has just been unfolded by a dozen of young engineers who had built and launched small experimental satellites called KITSAT-1 and KITSAT-2. Spacecraft technology is currently one of the most powerful weapons of many developed countries. Its importance is expected to be even bigger in the next generation. Although the spacecraft technology in Korea is far behind of other developed countries, its birth is now accelerating its growth to be a geostationary communication satellite, KOREA-SAT in 1996.

The main missions of currently operating satellites can be catagorised into three classes: communication, remote sensing, and scientific research. Above of all, the remote sensing from the satellite has been providing valuable information about the Earth; lands, ocean, and atmosphere. It gives enormous amount of information in a short period of time, which could not even be dreamed of by people who researched the Earth on the ground.

Many Korean scientists and engineers have been processing satellite images on their researches, which were taken by several remote sensing satellites such as Lansat, SPOT, METEOSAT and ERS-1. Since raw images from the satellite are very distorted geometrically and radiometrically, they have to be corrected before any applications. This correction step is generally called *pre-processing*. So far, we have only concentrated on the applications using already pre-processed images because we have not received data directely from any remote sensing satellites. However, as CCD cameras mounted in KITSAT A and B send image data and works on building a ground station which will receive remotely sensed data from other satellites are consistently carried on, the pre-processing has been regarded as the top priority job for the development of remote sensing technology in Korea.

In this paper, we present a geometric correction algorithm which is the most critical part of the pre-processing. The geometric correction algorithm proposed in this paper consists of two steps; (a) navigation of raw images (pre-correction) and (b) fine co-location of pre-corrected images using automatic tiepoint matching techniques.

The algorithm corrects raw, and hence, un-geolocated images from Along Track Scanning Radiometer(ATSR) working on ERS-1. First of all, the unfamiliar instrument ATSR is introduced briefly and some background about the geometric correction is reviewed in Section

2. In Section 3, the navigation and image geometry models for ATSR scanning process are mathematically derived. The pre-correction algorithm which is based on the navigation models is described. The geometrically pre-corrected images by this algorithm are shown. Section 4 describes the fine co-location algorithm using automatic coastline matching between two stereo views. This algorithm removes small geometric errors which cannot be corrected by the analytic navigation model. Finally, Section 5 concludes this paper and suggests the future approaches for the further development of this algorithm.

2 Background

2.1 Along Track Scanning Radiometer (ATSR)

The ATSR is a four channel infra-red radiometer used for measuring sea-surface temperatures (SST) and also cloud top temperatures. It was designed to provide the following types of data and observations: [1]

- SST with an absolute accuracy of better than 0.5K with a spatial resolution of $50km$ and in condition of up to 80% could cover
- images of surface temperature with $1km$ resolution and $500km$ swath, relative accuracy around 0.1K.

The measuring SST from space is two-fold: to devise and deploy a radiometer that is capable of the appropriate level of precision; and to correct for the effect of the intervening atmosphere, on account of molecular absorption, scattering and emission. This is achieved by three means:

- the ATSR is a multi channel device (12, 11, 3.7, $1.6\mu m$), and corrections can be inferred from the differing brightness temperatures measured by each channel, reflecting the spectral dependence of the atmospheric effects
- an innovative extension of this principle, whereby the surface is viewed at two angles, one close to the nadir(0^o) and the other at 47^o results in two measurements made with differing atmospheric path lengths, from which independent information is obtained about the effect of the intervening atmosphere

- using a passive microwave radiometer to measure the water vapour content of the atmosphere makes possible an even more precise determination of the temperature deficit, although less partially defined.

The geometric correction, does not concern about measurements of SST nor brightness values of a target. It depends only upon the image-taking method of the instrument, the scanning geometry, which determines the position of the instant field of view(IFOV) on the ground surface. Moreover, the scanning with two different look angles gives not only the independent information for the atmospheric corrections, but also a *stereoscopic view* of an imaged target. Therefore, the scanning method of the ATSR is detailed here.

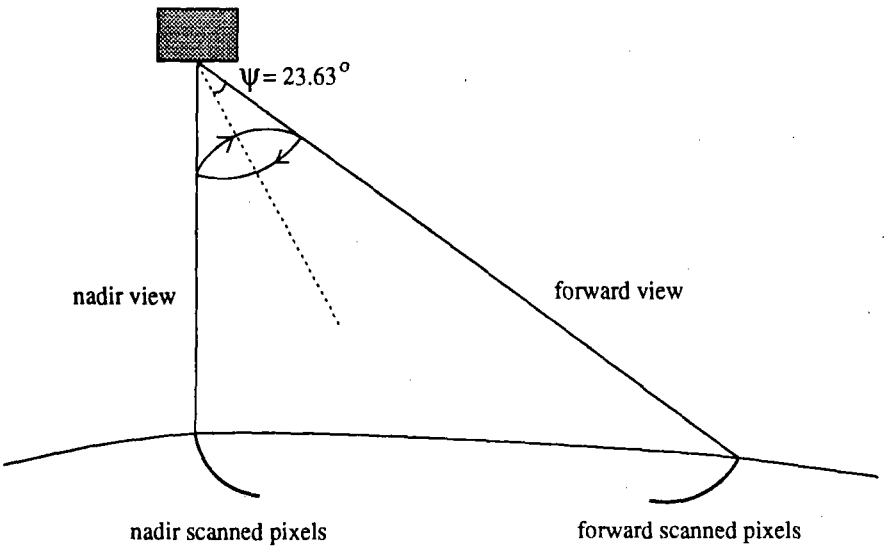

Figure 1: ATSR scanning process

The ATSR observes the Earth's surface along two curved swaths, these being the *nadir* (a nearly vertical path through the atmosphere) and *forward* (an inclined path) as shown in Figure 1. These swaths are produced by a scanning mirror with an axis of rotation inclined 23.63 ° from the vertical. Thus, the field of view by the instrument's detector via the scan mirror is a nearly elliptical path on the Earth's surface. However, not all of the scan is used to collect measurement from the surface, since it is interrupted by black body measurements. The scanning process by the scan mirror is shown in Figure 2.

In Figure 2, one scan takes $150msec$ and it is divided into 2000 pixels with an accuracy of 1/10 pixel. Therefore, one pixel duration time is $150msec/2000 = 75\mu sec$. To achieve the along track viewing and the swath coverage, a plane inclined mirror is continuously rotated to scan a cone of viewing vectors into the primary paraboloid. The scan mirror rotates clockwisely if looking from the satellite toward the ground. During one scan of 2000 pixels, 555 pixels are allocated for the nadir image, 371 pixels for the forward image. Two 16 pixels get the radiance from a cold and a hot black body each for the calibration of the image data. Nominally, both swaths are $500km$ in width, while the two views are separated by approximately $900km$ in along track distance.

The pixels making up the nadir views are normally 1×1 km. To meet this requirement, the instant angle of view became $1/777rads$ or 0.0737 °. The forward view pixels are larger, due to the viewing perspective and are about 1.5×2 km.

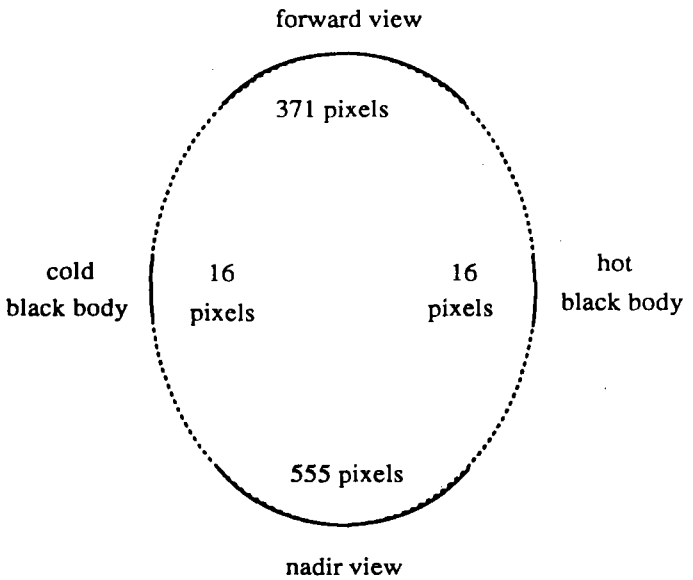

Figure 2: Footprint of a ATSR scan

2.2 Geometric Correction

Remotely sensed data usually contain both systematic and nonsystematic geometric errors. Figure 3 shows nadir and forward ATSR images before geometric correction. Large differences

in image form are observed. The errors may be divided into two classes:

- those that can be corrected using data from platform ephemeris and knowledge of internal sensor distortion
- those that cannot be corrected with acceptable accuracy without a sufficient number of *ground control points* (GCP).[1]

These geometric errors are well classified and summarised in [2].

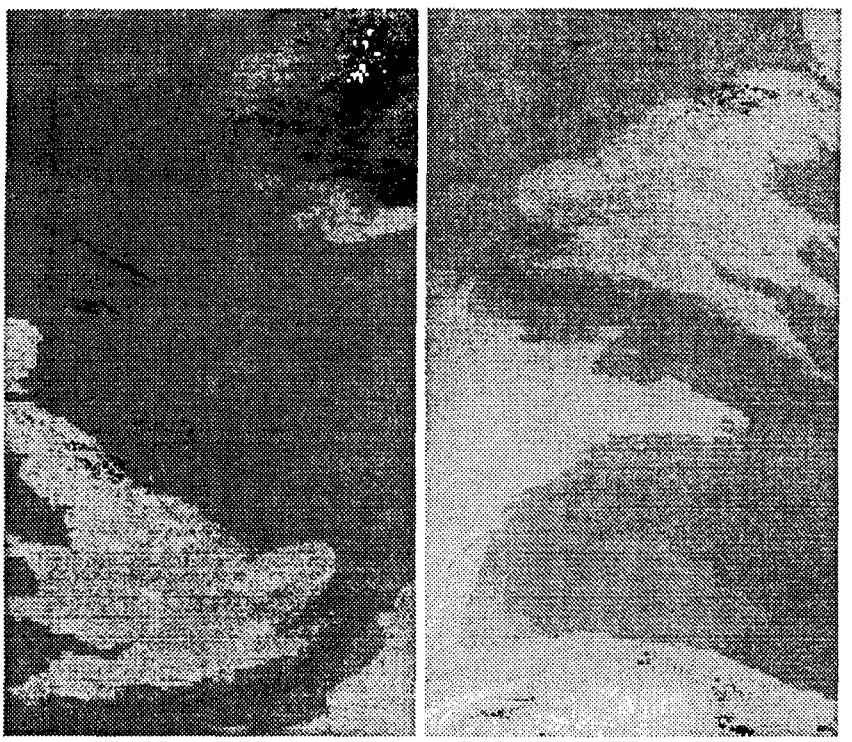

Figure 3: ATSR raw images: nadir(left) and forward(right) views

In the past, two methods have been used to attempt to correct the various types of geometric distortions in digital image data: (a) the nature and magnitude of inaccuracy sources were estimated and correction formulae were applied [3, 4, 5, 6, 7]; (b) the different coordinates

[1] A *ground control point*(GCP) is a point on the surface of the Earth where both image coordinates (measured in rows and columns) and map coordinates (measured in degrees of latitude and longitude, feet, or metres) can be identified.

between GCPs in an image and those on a map were used to derive mathematical relationships to correct the image geometry [8, 9, 10, 11]. Algorithms which combined these two methods were also proposed [12, 13].

The ATSR raw images collected by ERS-1, utilises a rotating mirror with an offset conical scan and has low resolution($1km \times 1km$). The conical scan produces circular distortions which prevent direct use of the correction method using GCPs. The mathematical models of the geometric correction differ from those for image data obtained from linear scanners [14, 15].

Because of its stereoscopic scans, the geometric correction of ATSR imagery is divided into two concepts: *geo-location* and *co-location*. The geo-location is the scheme by which nadir and forward pixels are put onto the right positions on the Earth's surface. The geo-located nadir and forward images, which are separated by about $900km$, are resampled to be in the same view. This is called co-location.

This paper presents both techniques discussed in this section; (a) an analytic correction model of the ATSR raw images (Section 3), (b) a fine co-location algorithm using the control points (Section 4). The overall geometric correction model proposed in this paper is illustrated in Figure 4. Ungeolocated (raw) ATSR images are corrected by a navigation model and these pre-corrected images are then finely co-located by removing small non-systematic errors to produce the corrected image.

3 Pre-correction by a Navigation Model

3.1 An Image Geometry Model of the ATSR

This section mainly describes how to derive the pixel positions scanned by the ATSR. This procedure requires very precise mathematical models for the ERS-1 orbit, its attitude states, scanning process, Earth's shape and its rotation.

Basically, a *vector projection method* is used to calculate the scanned pixel positions on the Earth surface. Cartesian coordinates are used for this procedure by virtue of its suitability for the vector projection method and rotation of axes.

Orbit prediction is one of the most difficult parts in ground segment processing due to the mathematically-complicated Earth's gravitational model. In addition, non-deterministic param-

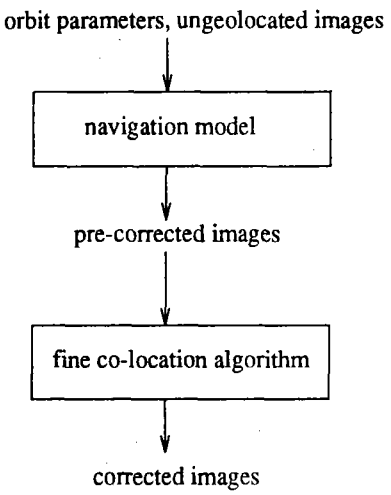

Figure 4: Overall geometric correction procedure

eters are important. An example is environmental perturbation - e.g. air drag, solar particle pressure, and Earth's electric/magnetic field. To date, many remote sensing organisations have devoted themselves to developing their own ERS-1 orbit determination systems. Therefore, it is beyond the scope of this paper. Practically, satellite state vectors at a certain time instant which is specified in the header of raw image data was obtained from one of ERS-1 orbit determination softwares.

Earth is formulated mathematically as an ellipsoid, and many pre-processing groups for remotely sensed image data accepted this Earth model as a compromise between its mathematical complexity and the similarity to the real Earth shape.

The pre-correction procedure is basically a sequence of coordinate transformations. First of all, a certain pixel position on the scanning cone is calculated in the coordinate system of the ATSR instrument itself. The pixel position has certain parameters in order to be generalised for all pixels on the scanning cone. The coordinate is then sequentially transformed into different coordinate systems, taking into account the scanning geometry and orbit-Earth model. Finally, the vector from the scan mirror to the pixel is projected onto the Earth surface in a geocentric coordinate system, and the position in along/across-track coordinates is then calculated by spherical triangle methods.

3.1.1 Coordinate on the Scanned Cone in Instrument Coordinate System

The scan mirror of the ATSR rotates around a reference axis which is tilted by α (23.63°). Figure 5 illustrates the instrument coordinate system ($X_a - Y_a - Z_a$) and a scanned point on the bottom circle of the cone. The Z_a axis is the reference axis of the imaginary cone. The Y_a-axis is perpendicular to the Z_a axis and directed to the centre pixel of the forward scan. The origin is located at the scan mirror (top of the cone).

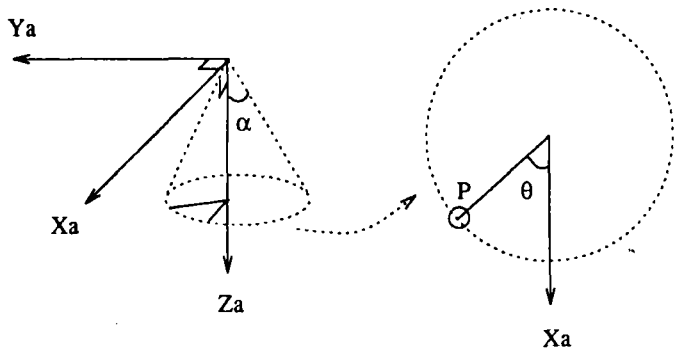

Figure 5: ATSR instrument coordinate system

In the $X_a - Y_a - Z_a$ system, the scanned vector is expressed as

$$P = (\sin\alpha\cos\theta,\ \sin\alpha\sin\theta,\ \cos\alpha). \tag{1}$$

3.1.2 Transformation to baseplate coordinate system

The baseplate axes ($X_b - Y_b - Z_b$) have its Z_b axis pointing to the nadir centre point. In other words, the instrument axes are mapped onto the baseplate axes by a rotation of α about the X_a axis.

The transformation matrix M_{ab} is,

$$M_{ab}(\alpha) = \begin{pmatrix} 1 & 0 & 0 \\ 0 & \cos\alpha & \sin\alpha \\ 0 & -\sin\alpha & \cos\alpha \end{pmatrix}. \tag{2}$$

3.1.3 Transformation to Platform Coordinate System

As the baseplate is not perfectly aligned to the platform ($X_p - Y_p - Z_p$), three successive rotations are required for correcting this misalignment. The transformation matrixes $M_x(\Delta z)$, $M_y(\Delta y)$,

$M_x(\Delta x)$ are:

$$
\begin{aligned}
M_z(\Delta z) &= \begin{pmatrix} \cos\Delta z & \sin\Delta z & 0 \\ -\sin\Delta z & \cos\Delta z & 0 \\ 0 & 0 & 1 \end{pmatrix} \\
M_y(\Delta y) &= \begin{pmatrix} \cos\Delta y & 0 & -\sin\Delta y \\ 0 & 1 & 0 \\ \sin\Delta y & 0 & \cos\Delta y \end{pmatrix} \\
M_x(\Delta x) &= \begin{pmatrix} 1 & 0 & 0 \\ 0 & \cos\Delta x & \sin\Delta x \\ 0 & -\sin\Delta x & \cos\Delta x \end{pmatrix}.
\end{aligned} \tag{3}
$$

3.1.4 Transformation to Earth Fixed Coordinate System

The ERS-1 attitude control system is based on two characteristics; [16]

1. The yaw axis points to the local vertical of the Earth.
2. The roll axis oriented along the composite ground velocity vector including Earth rotation.

The local vertical point on the Earth, $\vec{s} = (s_x, s_y, s_z)$ can be obtained by a fourth-order equation which is solved by a numerical method. It is described in Appendix A.

The unit vector $\vec{a} = (a_x, a_y, a_z)$ which is directed from $\vec{X}_{ers}$ (the position of the satellite in the Earth fixed frame) to $\vec{s}$ is, therefore,

$$\vec{a} = \frac{\vec{s} - \vec{X}_{ers}}{\|\vec{s} - \vec{X}_{ers}\|}. \tag{4}$$

The projection of the satellite velocity onto the plane perpendicular to $\vec{a}$ is

$$\vec{V}_p = \vec{V}_{ers} - (\vec{V}_{ers} - \vec{a})\vec{a}. \tag{5}$$

The velocity vector of the Earth rotation at $\vec{s}$ is

$$\vec{V}_{geo} = \frac{2\pi}{T}(-s_y, s_x, 0), \tag{6}$$

where T is a sidereal day. Therefore, the unit vector of the roll axis, $\vec{b} = (b_x, b_y, b_z)$, can be obtained by the relative velocity of the satellite to the Earth velocity;

$$\vec{b} = \frac{\vec{V}_{rel}}{\|\vec{V}_{rel}\|}, \tag{7}$$

where

$$\vec{V}_{rel} = \vec{V}_p - \vec{V}_{geo}. \tag{8}$$

The pitch axis, $\vec{c} = (c_x, c_y, c_z)$, is defined to be orthogonal to both $\vec{a}$ and $\vec{b}$;

$$\vec{c} = \vec{b} \times \vec{a} \tag{9}$$

Therefore, the transform matrix to the Earth fixed axes is[2]

$$M_E = \begin{pmatrix} c_x & b_x & a_x \\ c_y & b_y & a_y \\ c_z & b_z & a_z \end{pmatrix}. \tag{10}$$

3.1.5 Projection onto Earth's Surface

The vector pointing to the pixel is calculated by several transformations of P in Equation 1.

$$\begin{aligned} M &= (m_1, m_2, m_3) \\ &= M_E M_x(\Delta x) M_y(\Delta y) M_x(\Delta z) M_{ab}(\alpha) P. \end{aligned} \tag{11}$$

The equation of the line of the pixel vector is

$$(x, y, z) = a(m_1, m_2, m_3) + (X_s, Y_s, Z_s), \tag{12}$$

where (X_s, Y_s, Z_s) is the position vector of the satellite in the Earth fixed frame, and a is a variable. The equation of the Earth ellipsoid is

$$\frac{x^2 + y^2}{R_e} + \frac{z^2}{R_p} = 1, \tag{13}$$

where R_e is the length of major axis of Earth ellipsoid and R_p is that of minor axis. The solution of Equation 12 and 13 is

$$a_p = \frac{-B - \sqrt{B^2 - AC}}{A}, \tag{14}$$

where

$$\begin{aligned} A &= (m_1^2 + m_2^2)R_p^2 + m_3^2 R_e^2 \\ B &= (m_1 X_s + m_2 Y_s)R_p^2 + m_3 Z_s R_e^2 \\ C &= (X_s^2 + Y_s^2)R_p^2 + Z_s^2 R_e^2 - R_e^2 R_p^2. \end{aligned} \tag{15}$$

[2]The inverse of an orthogonal matrix is its transpose.

The coordinates (x_p, y_p, z_p) of the pixel point on the Earth surface is, therefore,

$$\begin{aligned} x_p &= X_s + a_p m_1 \\ y_p &= Y_s + a_p m_2 \\ z_p &= Z_s + a_p m_3. \end{aligned} \tag{16}$$

Pixel latitude and longitude are calculated according to the formula:

$$\begin{aligned} \text{latitude} &= \tan^{-1}\left(\frac{z_p}{\sqrt{x_p^2 + y_p^2}}\right) \\ \text{longitude} &= \tan^{-1}\left(\frac{y_p}{x_p}\right). \end{aligned} \tag{17}$$

3.1.6 Along- and Across-track Distances

Latitude-longitude display is not suitable for an inclined orbit because shape and scale of images compared with those measured on ground varies according to the latitude of the sub-satellite point. Finally, the pixel positions in Earth's fixed coordinates are represented in a x (across-track) and y (along-track) plane. The along-track direction is defined to be parallel to the velocity vector of the sub-satellite point relative to a fixed Earth. The across-track coordinate is then measured along the great circle orthogonal to the sub-satellite track [17]. The conversion is based mainly on the properties of a spherical triangle [18].

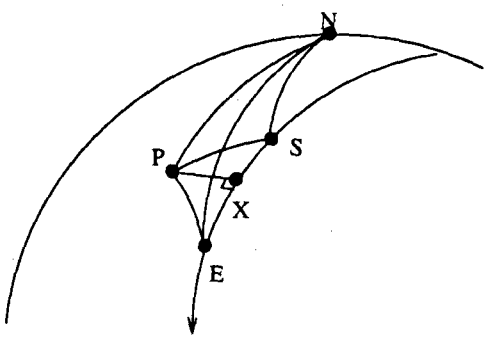

Figure 6: Spherical geometry of sub-satellite track and a scanned pixel

Figure 6 is showing southbounding sub-satellite points and a scanned pixel point (P) on Earth's surface. The line between S and E is a part of sub-satellite track which is short enough

to be approximated to be an arc[3]. X is the point between S and E at which the great circle joining P is orthogonal to the track.

In the spherical triangle $N - S - E$,

$$\begin{aligned} Side(NS) &= 90 - S_a \\ Side(NE) &= 90 - E_a \\ Angle(SNE) &= S_o - E_o, \end{aligned} \tag{18}$$

where the subscripts a and o represent latitude and longitude respectively. By using these three known parameters and the sine law [18], all six parameters (3 angles and 3 sides) of the triangle can be calculated. We can also solve the triangle $S - N - P$ by the same method using the latitude and longitude of the pixel.

To find the position of X, we first solve the triangle $P - S - E$.

$$Side(PS) = \cos^{-1}(\sin P_o \sin S_o + \cos P_o \cos S_o \cos(P_a - S_a)), \tag{19}$$

by which other two sides can be calculated as well. The angle PES can be also calculated by the cosine rule [18]:

$$Angle(PES) = \cos^{-1}\left(\frac{\cos(Side(PS)) - \cos(Side(PE))\cos(Side(SE))}{\sin(Side(PE))\sin(Side(SE))}\right). \tag{20}$$

The side P_X and X_E, which determine the position of X and along/across track distances of P, can be acquired by Napier's laws by virtue of the orthogonality of the triangle $P - E - X$:

$$\begin{aligned} Side(PX) &= \sin^{-1}(\sin(Angle(PES)) \times \sin(Side(PE))) \\ Side(XE) &= \cos^{-1}(\cos(Side(PE))/\cos(Side(PX))) \end{aligned} \tag{21}$$

Therefore, the final coordinates (x, y) of the pixel P in along/across track domain are

$$\begin{aligned} x &= Side(PX) \times R_e \\ y &= (Y(E) - Side(XE)) \times R_e \end{aligned} \tag{22}$$

where $Y(E)$ is y-coordinate of E.

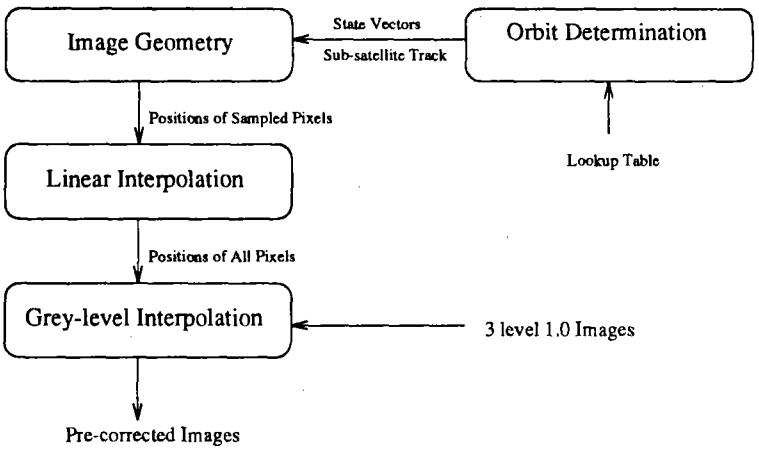

Figure 7: Block diagram of the pre-correction algorithm

3.2 Algorithm and Software

The pre-correction algorithm is illustrated in Figure 7. All modules except an orbit determination part were programmed in ANSI-C language in UNIX system. The orbit determination module was programmed in C language in VAX/VMS system in RAL[4].

Since the nadir and forward images in non-co-located images are separated by about $900km$, at least three consecutive raw images are required to give two co-located images[5].

The orbit determination programme linked an object file called ERSORB.OLB[6] and a lookup table which contains state vectors at the orbit ascending nodes. The image geometry module receives orbit information from the orbit determination module including state vectors (position and velocity) of the satellite and Kepler's elements at the image acquisition time and sub-satellite latitudes/longitudes. Attitude steering angles were calculated using those orbital information. Misalignment angles were acquired from experimental data in RAL.

Along/across track coordinates of pixels are calculated in the image geometry module which is based on the image geometry model in the previous section. Since this module has many matrix multiplications and trigonometric functions, only the coordinates of the first scan

[3]In practice, sub-satellite track is not an arc (part of great circle) due to Earth's rotation.
[4]Rutherford Appeleton Laboratory in UK is currently processing ATSR images.
[5]One raw image consists of 560 scans.
[6]This ERS-1 orbit determination software was developed by European Space research and TEchnology Centre(ESTEC).

of each raw image were calculated. Those of the rest of the scans were linearly interpolated in the next module.

Finally, grey-values of the raw images are interpolated into the corrected images by means of a nearest neighbourhood interpolation technique [19]. The pre-corrected images are 512×512 geo- and co-located IR count images (nadir and forward).

3.3 Results and Conclusion

Three consecutive raw images have already been shown in Figure 3. Both views are severely distorted: concave- and convex-shaped due to the elliptical scans. They are not co-located ($900km$ separation) and the forward image is flipped because the scanning directions of the nadir and forward views are opposite.

Figure 8 shows the pre-corrected images of Figure 3. They are geo-located, co-located, and displayed in along/across-track coordinates.

Figure 8: Pre-corrected images: nadir(left) and forward(right) views.

The corrected nadir and forward images were thresholded and their differences were compared in Figure 9. The figure shows the residual geometric errors between two views.

This section dealt with the pre-correction of ATSR raw images using the image geometry. The camera model was derived mathematically and the algorithm was developed. The results showed some co-location errors and these errors are not the ones which can be removed by the analytic method. These errors are caused mainly by five sources; attitude variation, positional

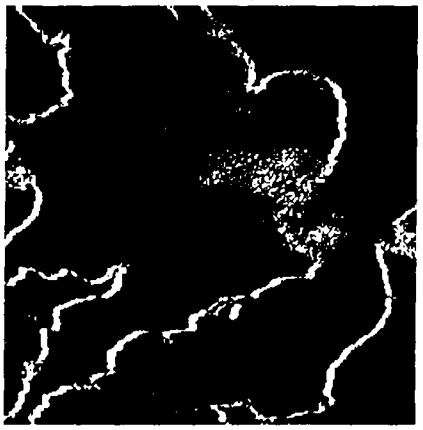

Figure 9: The difference of pre-corrected nadir and forward images (thresholded) resulted from the proposed pre-correction algorithm

inaccuracy of the satellite, deviation of real Earth shape from the ellipsoid, sampling time error, and atmospheric refraction [20]. A fine-correction algorithm is described in the next section in order to minimise these small errors.

4 Fine Co-location of ATSR Images

This section describes the accurate co-location of pre-corrected ATSR images. This technique reduces geometric errors between two views to $\pm 1km$. This allows stereoscopic information to be obtained on images of clouds to enable their height to be determined automatically [21].

The technique uses coastlines in two views as tiepoints. Coastlines are suitable objects on the Earth surface which are invariant with time and well distinguished in a $1km \times 1km$ resolution image. In addition, they are located at sea surface level so that they should not show any disparity in stereo pictures. Binary cross-correlation matching algorithms were used to determine the positional relationship between coastline images in both forward and nadir directions. A general interpolation technique was applied using polynomial warping to obtain a least-square fit.

O'Brien and Turner[13] modified a navigation model of AVHRR images by using coastlines. Unfortunately, they registered the map coastline images into the raw image domain by the inverse navigation model and compared them with raw coastline images. This method is inadequate for

co-locating nadir and forward images in the present case of ATSR data. The opposite effects of elliptical distortion in two views (concave and convex) leads to an unacceptable inaccuracy. It is necessary that an intermediate pre-corrected image domain should be adopted and coastlines in both views should be compared in this domain as shown in Figure 3.2.

Their algorithm was applicable only for a connected concave coastline. In practice, coastline segments can be separated by clouds or the edges of an image. In addition, they selected the centroid of the coastal points as the origin of rotational errors. This does not take into account the reason for the rotational distortions - attitude variations of the satellite cause the rotational effects in images and so the origin of rotation must be related to the position of satellite.

The proposed algorithm overcomes these problems by using an improved algorithm and by the unique characteristics of the co-location rather than geo-location.

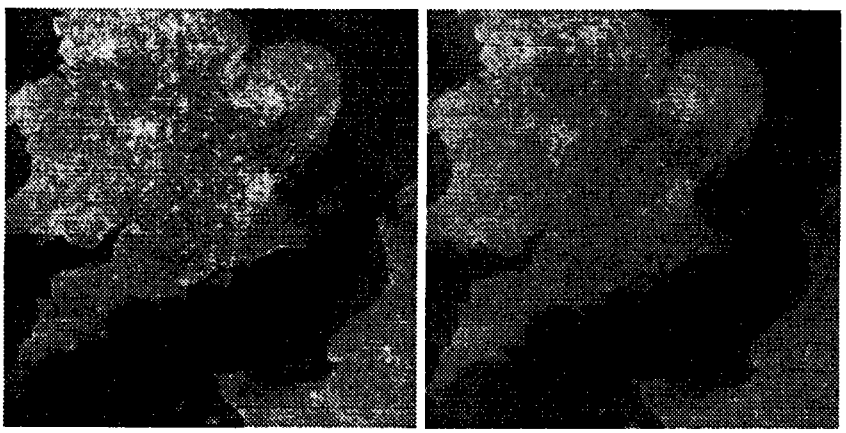

Figure 10: Original pre-corrected nadir(left) and forward(right) views

4.1 Coastline Detection

The present work used summer and/or day-time images when lands are hotter than sea. They were RAL pre-corrected brightness temperature(BT) image products[7]. Images were 512 by 512 pixels in size. They were geo-located and co-located (only pre-corrected from the point of view of this paper) nadir and forward BT images from the available ATSR channels (1.6, 3.7, 11, 12

[7]The proposed algorithm utilises BT variations of sea. Since the current study does not involve the radiometric correction to convert IR counts to BT, the pre-corrected image from RAL rather than from the proposed pre-correction algorithm was used for the current research.

μm) [17]. Unfortunately, the $11\mu m$ and $12\mu m$ of the ATSR data are not aligned precisely with each other and show about 0.1 pixel deviation. This effect is serious especially around cloud edges and coastlines. Therefore, multi-channel properties were not able be used to detect the coastlines.

The temperature difference between land, sea and cloud was used to identify and segment images into three regions using the $11\mu m$ channel thermal IR images. Difficulties arose to determine general thresholds between the regions for various imaging times and places. Rather than using a large amount of experimental database for these thresholds, the fact was used that sea is spatially uniform during the day. The temperature difference of two neighbouring pixels on the sea is less than $0.3 - 0.4K$. This threshold is almost independent of the imaging time and place. Interconnected pixels corresponding to images of the sea were used as a segmentation technique.

The 4-*connectivity* algorithm [19] was used for segmentation. Figure 10 shows the original pre-corrected images and Figure 11 shows boundaries between all different groups. The forward view shows more uniform temperature distribution due to its lower resolution.

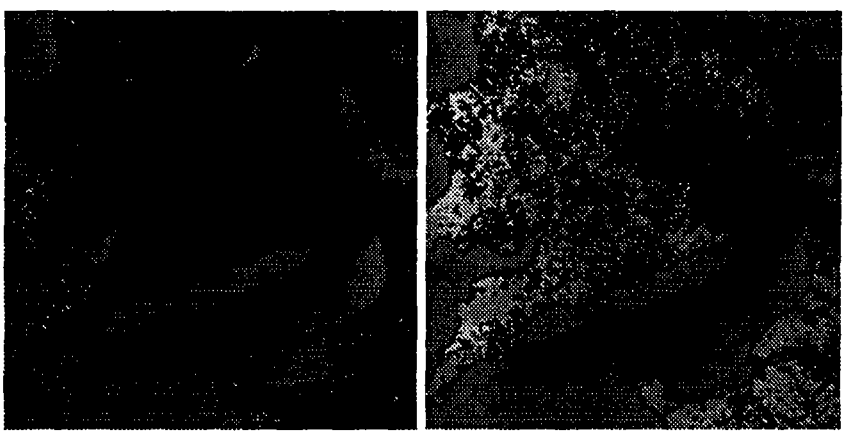

Figure 11: Boundaries between all different groups: nadir(left), forward(right)

The following procedure is used to find groups with more than 1000 pixels. These are named *big groups*. A typical histogram of temperatures during the day is shown in Figure 12. This figure shows the temperature distribution of the original images and averaged temperature distributions of the big groups. Although the histogram is continuous, the big groups can be

seen to be divided into a maximum of three temperature bands. This number of bands depends on whether the image contains large areas of sea, land and cloud. The averaged temperatures of the big groups are displayed with the histograms which have two peaks (land and sea) and a tail (cloud).

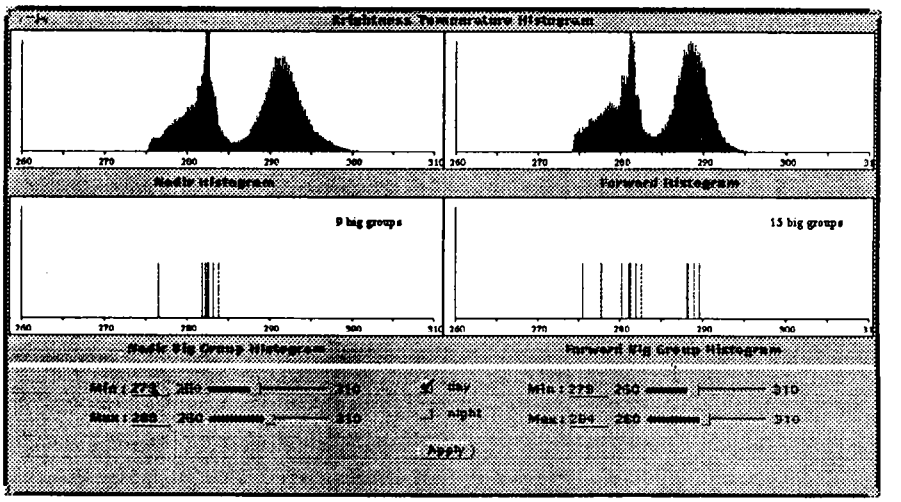

Figure 12: Histograms and big group bands

During the summer and/or daytime, sea is colder than land and hotter than clouds. Therefore, two approximate thresholds (upper against land and lower against clouds) are automatically set in order to maximise class separability [22] and extract big sea groups (see two thresholds in Figure 12). If these thresholds do not extract the big sea groups, correct thresholds are manually set. Boundaries of the big sea and land groups of pixels, which contact to and have higher temperatures than those big sea groups, are identified as coastlines as shown in Figure 13. It can be seen that clearly connected coastlines without cloud edges and edges over land can be observed.

The result of this procedure was to obtain two binary images (nadir and forward views) of coastline pixels.

4.2 Coastline Matching (Binary Cross-correlation)

The coastlines in the nadir image were chosen as a reference for the co-location algorithm to be described. In order to match the coastlines of two views, pieces of coastline in the forward

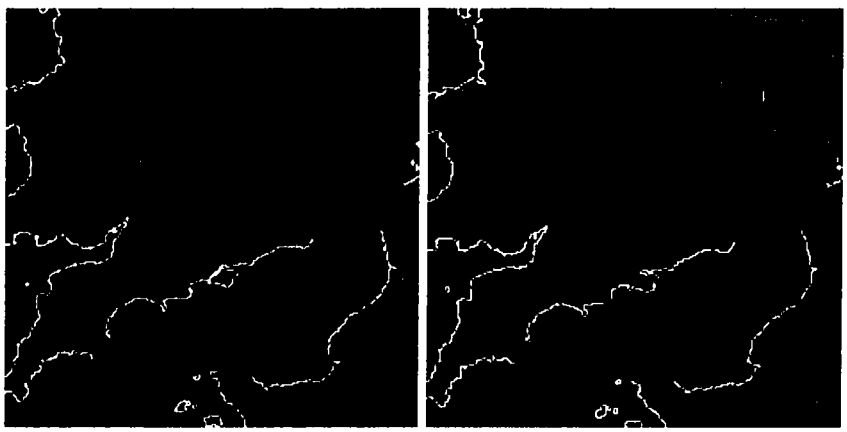

Figure 13: Coastline images: nadir(left), forward(right)

image are shifted both horizontally and vertically. The binary cross-correlation for each amount of shift was:

$$C(i,j) = \sum_{y}\sum_{x} N(x,y)F(x+i,y+j), \quad for \ -n < i < n \ , \ -m < j < m \qquad (23)$$

where n is a maximum horizontal deviation, m is a maximum vertical deviation, $N(x,y)$ and $F(x,y)$ are the binary nadir and the forward images respectively at image coordinate (x,y). The $N(x,y)$ is the coastline image of the whole nadir image, but $F(x,y)$ is part of forward coastline image. The ranges of x and y depend on the sectioning method used for coastline images in the forward view: *fixed-length section* and *variable-length section.*

After calculating $C(i,j)$ for each i and j, i_{max} and j_{max} were calculated to produce the largest correlation $C_{max}(i_{max}, j_{max})$. Finally, those coastlines were regarded as matched tiepoints if the C_{max} was larger than a certain threshold.

This algorithm corrected for both displacement and rotational errors. In general, a reference point (which is the origin of the rotation) is required to find the rotational effects. The origin of the rotation cannot be one point in one image due to the time-varying attitude variations while scanning the image. This fact also suggests the existence of higher order non-linear distortions in the image. In the algorithm, the coastlines were sectioned and shifted a different amount for each section. This algorithm allowed not only for global rotational distortions but also the spatially non-linear distortions.

Two different algorithms were compared as methods for sectioning the forward view coastlines:

Fixed length sectioning

1. Coastline sections in the forward image were made of equal length(12 pixels)
2. Each section was shifted horizontally and vertically within maximum deviations($\pm$10 pixels)
3. The amount of shift in each direction was determined which gave the maximum correlation with the nadir coastline
4. If the maximum correlation was larger than a threshold of 8 pixels, the positions of the matched pixels were stored as inputs and desired outputs for finding a transfer function.

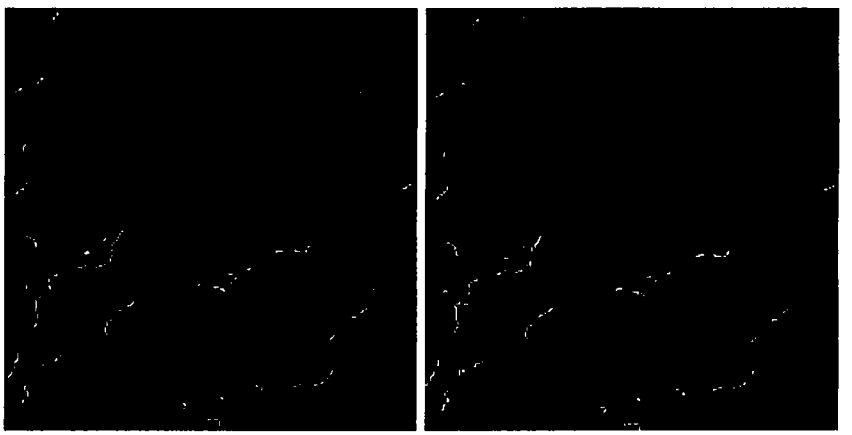

Figure 14: Matched pixels by the fixed length sectioning method: Nadir(left), Forward(right)

Variable length sectioning

1. The positions of each group of connected pixels of the forward coastline image were stored as a section
2. Each section was shifted to produce the maximum correlation in forward and nadir view
3. The group of matched pixels was found which was longer than a threshold of 2 pixels

4. Their positions were stored and ignored in subsequent processing

5. Steps 1) - 4) were repeated until no more coastline group was accepted

It was found that the fixed length sectioning of a coastline generated errors because the matching correlation depended on the initial starting point of sections. However, it was faster than the variable length sectioning algorithm which had a variable size of memory allocation for each section and repeated several times. Figure 14 and 15 show the matched coastline pieces by using each method. The length of 12 pixels and the matching threshold of 8 pixels were found to be adequate to the fixed length sectioning algorithm. The variable length sectioning algorithm used 3 pixels for the acceptance length. This length was sufficient to exclude false matched pairs.

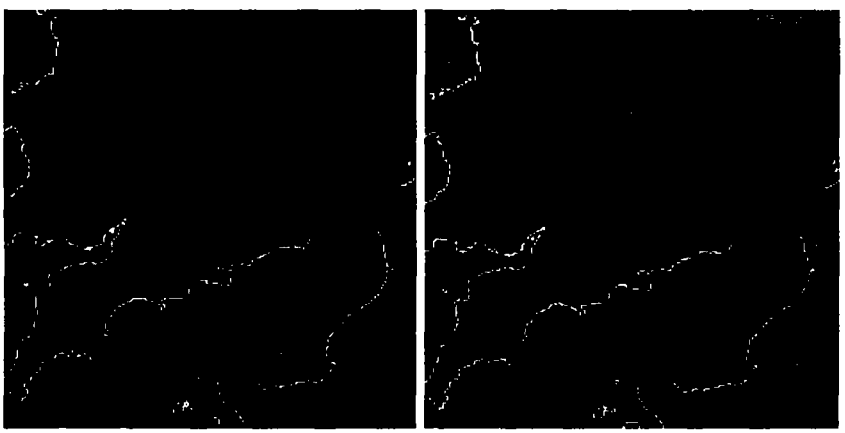

Figure 15: Matched pixels by the variable length sectioning method: Nadir(left), Forward(right)

4.3 Interpolation

Transfer functions were obtained to describe the relationship of matched tiepoints. First order polynomials were selected as transfer functions. The reasons for this were: (a) tiepoints are not uniformly distributed across the images, and (b) the images had already been pre-corrected. Non-linear characteristics of high order polynomials cause extra distortion. Moreover, the lower order polynomial functions increased the processing speed.

The polynomials used were :

$$x_o = a_0 + a_1 x_i + a_2 y_i \qquad (24)$$
$$y_o = b_0 + b_1 x_i + b_2 y_i$$

where (x_o, y_o) and (x_i, y_i) are the coordinate of the forward image domain before and after the correction respectively. In order to calculate the coefficients of the polynomials (a's and b's) with more than three matched tiepoint coordinate pairs, the least square fitting algorithm was used.

An iteration algorithm was used to exclude those tiepoints which were more than ± 1 pixel from the positions obtained by the polynomials and new polynomials were calculated with the remained tiepoints.

The polynomial warping was now applied to the forward image using the *nearest neighbour interpolation* method. This algorithm is simple, fast, and does not change radiometric information of the image. Figure 16 shows the corrected forward image by warping using tiepoints with the fixed length sectioning method.

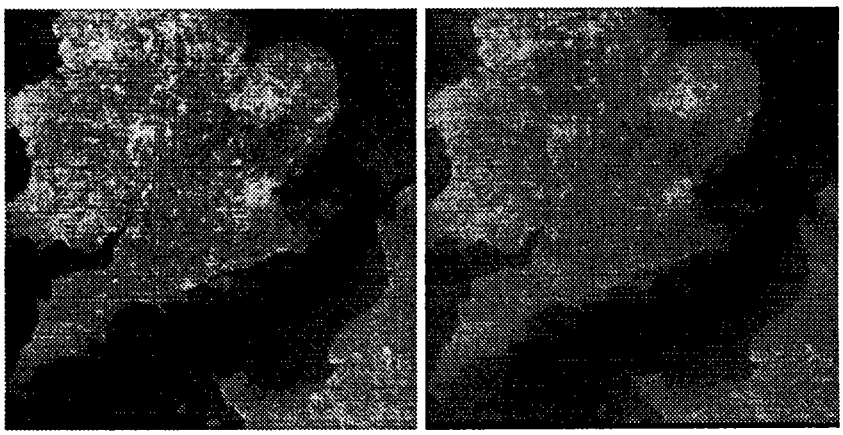

Figure 16: Finely co-located images by fixed length sectioning method: original nadir(left), corrected forward(right)

4.4 Results and Conclusions

Figure 17 shows the co-location errors of the original images and those of the corrected images by using the fixed length sectioning algorithm.

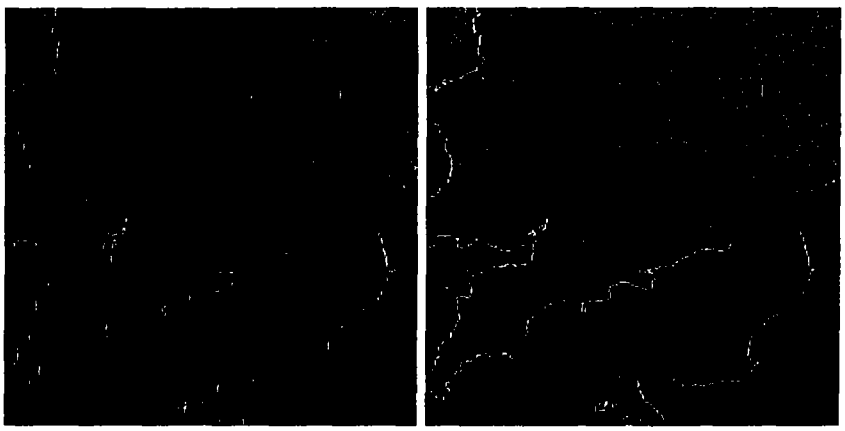

Figure 17: Co-location errors: original(left), corrected by fixed length sectioning method(right)

The performance of the proposed algorithm was numerically assessed by an ***adaptive least square matching***(ALSM) algorithm [23]. This technique is one the most accurate matching algorithms for regions with continuous disparity. Coastline pixels of the nadir view in the original and corrected images are selected for the matching assessment. Since a coastline is not a disparity discontinuity but grey-level discontinuity, this assessing algorithm was regarded as the most reliable method. Geometric error was the distance of x- and y-disparities between the nadir and forward views. Mean error, maximum error, and the number of pixels used for the assessment are summarised in Table 1.

Image1 (400)				
	original	fixed-section	variable-section	patch-based
mean error (pixels)	6.147	1.066	0.853	0.810
max error (pixels)	7.660	2.382	2.351	2.722
number of pixels used	441	472	522	528

Table 1: Numerical results of each algorithm

The patch based cross-correlation algorithm (Lemmen 1988) was implemented to be compared with the binary correlation algorithms. The window size of 15×15 was used. It did not give much better results though it took $15 \times 15 \times 12 = 2700$ times longer processing time than the fixed length sectioning algorithm. This algorithm gave even worse results when patches had disparity discontinuity which was caused by presence of clouds in the image.

The fine co-location of the pre-corrected ATSR images using coastlines was described in this section. The proposed algorithm is automatic and it aims at maximising processing speed. The efficiency of the fixed length sectioning and the variable length sectioning algorithms were compared. The finely co-located images reduced the positional error to ± 1 km by both algorithms.

Since the proposed algorithm employs the polynomial warping technique, the tiepoints need to be well spread over the image frame. In practice, this algorithm is not favourable for the image frames in which not enough coastline pixels are detected due to either geophysical location or severe cloud occlusion.

5 Conclusion and Further Development

This paper proposed a comprehensive geometric correction algorithm of ATSR raw images by two folds; (a) the pre-correction algorithm using image geometry and orbital models (Section 3), and then (b) the fine co-location algorithm using the binary cross-correlation (Section 4). The camera model was derived mathematically and the algorithm was developed in codes. The results showed some co-location errors between nadir and forward views. These non-systematic errors were then minimised by the fine co-location algorithm. The fine co-location algorithm detected coastlines in images by a region segmentation technique. The detected coastline pixels were automatically correlated by two binary cross-correlation techniques. The polynomial warping was applied reducing the non-systematic errors to ± 1 pixel.

The polynomial warping is regarded as the biggest drawback in the whole algorithm. It does not model geometric error sources, and hence, it requires a large number of, well-spread tiepoints. The works on a new system which represents geometric error sources rather than the polynomials are being carried on. This is basically to estimate internal parameters (position, velocity and attitude of the satellite) using an optimisation technique, extended Kalman filter. It is expected to perform more accurately than the polynomial warping technique with much less number of tiepoints.

A Local Vertical Sub-satellite Point

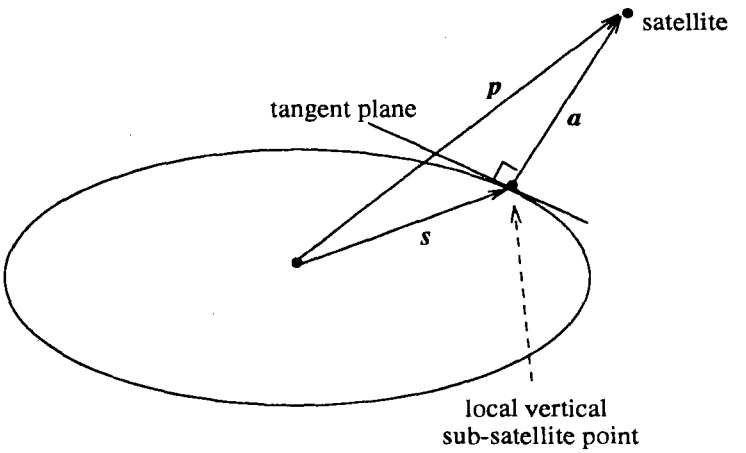

Figure 18: Ellipsoidal Earth

Figure 18 shows a local vertical sub-satellite point(SSP) on the ellipsoidal Earth. Since the polar axis, satellite position vector $\vec{p}$ and the local vertical SSP vector $\vec{s}$ are co-planar, the geometry was simplified to a two dimensional model.

Let $\vec{s} = (s_x, s_y)$ and $\vec{p} = (p_x, p_y)$. The condition that the point (s_x, s_y) lies on the Earth's ellipse gives:

$$\frac{s_x^2}{R_e^2} + \frac{s_y^2}{R_p^2} = 1, \tag{25}$$

where R_e and R_p is equitorial radius and polar radius respectively. By using the gradient of the above equation, the normal vector at the local vertical SSP, $\vec{a}$, can be obtained:

$$\vec{a} = k(\frac{s_x}{R_e^2}, \frac{s_y}{R_p^2}), \tag{26}$$

where k is a constant. Since $\vec{a} = \vec{p} - \vec{s}$, Equation 26 gives the relationship:

$$\begin{aligned} p_x - s_x &= k\frac{s_x}{R_e^2} \\ p_y - s_y &= k\frac{s_y}{R_p^2}. \end{aligned} \tag{27}$$

Elimination of the constant k gives [16]:

$$R_e^2\frac{p_x - s_x}{s_x} = R_p^2\frac{p_y - s_y}{s_y}. \tag{28}$$

Equation 25 and 28 are solved by numerical methods for s_x and s_y.

References

[1] Vass P and M Handoll, "*UK ERS-1 Reference Man ual (DC-MA-EOS-ED-0001)*", Earth Observation Data Centre (EODC), January 1991.

[2] Shin D, "*On the review of satellite imagery geometric correction*", VeKNI Bericht zum 20 jahrigen Bestehen, 1993.

[3] Brush R J H, "*A method for real-time navigation of AVHRR imagery*", IEEE Transactions on Geoscience and Remote Sensing, **GE-23**, No.6, 876-886, 1985.

[4] Brush R J H, "*The Navigation of AVHRR Imagery*", International Journal of Remote Sensing, **9**, No.9, 1491-1502, 1988.

[5] Wolff T, "*An image geometry model for METEOSAT*", International Journal of Remote Sensing, **6**, 1599-1606, 1985.

[6] Brunel P, and A Marsouin, "*An operational method using ARGOS orbital elements for navigation of AVHRR imagery*", International Journal of Remote Sensing, **8**, No.4, 569-578, 1987.

[7] Straka J, J Klokocnik, and H Grabel, "*Navigation of satellite measurements without ground control points*", International Journal of Remote Sensing, **14**, 1981-2003, 1993.

[8] Benny A H, "*Automatic relocation of ground control points in Landsat imagery*", International Journal of Remote Sensing, **4**, No.2, 335-342, 1983.

[9] Davison G J, "*Ground control pointing and geometric transformation of satellite imagery*", International Journal of Remote Sensing, **7**, No.1, 65-74. 1986.

[10] Leeuw A J De, L M M Veugen, and H T C Van Stokkom, "*Geometric correction of remotely-sensed imagery using ground control points and orthogonal polynomials*", International Journal of Remote Sensing, **9**, 1751-1759, 1988.

[11] Novac K, "*Rectification of digital imagery*", Photogrammetric Engineering and Remote Sensing, **58**, 339-344, 1992.

[12] Cracknell A P and K Paithoonwattanakij, "*Pixel and sub-pixel accuracy in geometrical correction of AVHRR imagery*", International Journal of Remote Sensing, **10**, No.4-5, 661-667, 1989.

[13] O'Brien D M and P J Turner, "*Navigation of coastal AVHRR imagery*", International Journal of Remote Sensing, **13**, 509-514, 1992.

[14] Malhotra R C, "*Geometric Evaluation of Skylab S-192 Conical Scanner Imagery*", Photogrammetric Engineering and Remote Sensing, **43**, 169-182, 1977.

[15] Murphery S W, R D Depew, and R Bernstein, "*Digital Processing of Conical Scanner Data*", Photogrammetric Engineering and Remote Sensing, **43**, 155-167, 1977.

[16] O'Brien D M and A J Prata, "*Navigation of ERS-1 Along-Track Scanning Radiometer (ATSR) Images*", ESA Journal, **14**, 447-465, 1990.

[17] Bailey P, "*SADIST Products (Version 500)*", Rutherford Appeleton Laboratory(RAL), June 1993.

[18] Wertz J R, "*Spacecraft Attitude Determination and Control*", Kluwer Academic Publishers, 1978.

[19] Gonzalez R C and R E Woods, "*Digital Image Processing*", Addison-Wesley, 1992.

[20] Shin D, "*Application of Machine Vision to Cloud Studies using Stereoscopic Satellite Images*", Transfer thesis, Elec. Eng. Dept., University College London, 1994.

[21] Lorenz D, "*On the feasibility of cloud stereoscopy and wind determination with the Along-Track Scanning Radiometer*", INT. J. Remote Sensing, **6**, No.8, 1445-1461, 1985.

[22] Otsu N, "*A threshold selection method from grey-level histograms*", IEEE Transactions on System, Man, and Cybertics, **SMC-9**, 62-66, 1979.

[23] Gruen A W, "*Adaptive Least Square Correlation: A Powerful Image Matching Technique*", S. Afr. Journal of Photogrammetry, Remote Sensing and Cartography, **14**, No.3, 1985.